separations

MDPI

Review

Fabrications and Properties of Heteroatom-Based Co-Doped Biochar for Environmental Application: A Review

Meizhi Yang [1,†], Suxing Luo [2,3,*,†], Ping Zeng [3,4] and Yuanhui Wu [2,3,*]

[1] Department of Research and Development, Guizhou Open University, Guiyang 550023, China; meizhiyang01@163.com
[2] School of Chemistry and Chemical Engineering, Zunyi Normal University, Zunyi 563006, China
[3] Special Key Laboratory of Electrochemistry for Materials of Guizhou Province, Zunyi 563006, China; zengping2025@163.com
[4] School of Resources and Environment, Zunyi Normal University, Zunyi 563006, China
* Correspondence: suxingluo@126.com (S.L.); yhwull@126.com (Y.W.)
† These authors contributed equally to this study.

Abstract: For the past few years, biochar has emerged as a promising material for the removal of various pollutants from aquatic environments, owing to its advantageous characteristics, such as tunable porosity, abundant surface functional groups, ease of modification, and relative stability. Co-doping biochar with heteroatoms significantly enhances its surface properties by introducing additional functional groups and surface defects, which facilitate the adsorption and catalytic degradation of pollutants. This review conducts bibliometric analyses of relevant publications, synthesis methodologies, applications, and reaction mechanisms of co-doped biochar as an adsorbent and catalyst for contaminant removal, due to the synergistic effects of doping elements and biochar features. Furthermore, co-doping strategies and associated properties including specific surface area (SSA), surface functional groups, and defects of biochar are analyzed. Finally, future research directions are proposed to improve the efficiency of biochar in water and soil remediation applications. In summary, this review advances the frontier of research on heteroatom-based co-doped biochar and offers new insights into strategies for effective contaminant removal.

Keywords: co-doped biochar; biomass; heteroatoms; adsorption; activation oxidation

Academic Editors: Adrian Bonilla-Petriciolet, Didilia Ileana Mendoza-Castillo and Hilda Elizabeth Reynel-Ávila

Received: 6 January 2025
Revised: 15 January 2025
Accepted: 19 January 2025
Published: 22 January 2025

Citation: Yang, M.; Luo, S.; Zeng, P.; Wu, Y. Fabrications and Properties of Heteroatom-Based Co-Doped Biochar for Environmental Application: A Review. *Separations* **2025**, *12*, 20. https://doi.org/10.3390/separations12020020

1. Introduction

Biochar is a solid carbon-rich material produced through thermochemical conversion processes, such as hydrothermal carbonization and pyrolysis, from various bio-wastes [1,2]. It serves as a bridge between waste management and resource recovery. This dual role, as a waste-derived material and a functional product, aligns closely with global efforts toward carbon neutrality and circular economy goals. As a sustainable material derived from biomass, biochar offers notable advantages including high porosity, abundant surface functional groups, simple preparation processes, and low cost due to the wide range of raw material choices (e.g., sawdust, lignin, sewage sludge, and cow dung). These features have attracted considerable attention to biochar's potential for addressing environmental and energy challenges, particularly as an adsorbent, catalyst, and electrochemical energy storage material [3–5].

In previous studies, pristine biochar was directly applied for environmental remediation without further modifications [3,6,7]. However, pristine biochar often suffers from

low efficiency and limited applicability due to its relatively simple structure and limited functional diversity [1,8]. To address these limitations, modification strategies have been extensively explored, with heteroatom doping (e.g., N, S, P, and O) proving particularly effective. Heteroatom doping can remarkably change the characteristics of biochar, introducing structural defects, activating functional groups, and modifying the degree of graphitization, which collectively enhance its performance [9–11]. In some cases, the N-doped biochar has demonstrated an adsorption capacity exceeding tenfold that of the pristine biochar [12]. Furthermore, many publications highlight the synergistic effects of heteroatom-based co-doped biochar. The simultaneous incorporation of at least one heteroatom into biochar [13] introduces additional structure defects, surface functional groups, and active sites, enhancing porosity and overall performance compared to single-doped biochar [14]. These synergistic modifications can further promote the biochar's pollutant removal capacity. Xiao et al. [15] utilized N, P co-doped biochar to adsorb CO_2, achieving a capacity of 5.31 mmol/g at 500 kPa and maintaining 100% of the initial adsorption capacity after 20 cycles. This excellent performance was mainly attributed to the synergistic effect between N and P atoms and the additional active sites introduced during the process.

Given the limitations of pristine and single-doped biochar in meeting the current demands for pollutant adsorption and degradation, the development of heteroatom-based co-doped and even multi-doped biochar has become an inevitable trend. Selecting an appropriate doping strategy for specific pollutant removal requires careful trade-offs among various physicochemical properties, such as heteroatom content, specific functional groups, degree of graphitization, and pore volume, as these factors significantly impact removal efficiency. However, existing research articles and review papers lack comprehensive summaries on the preparation strategies, performance optimization, and application mechanisms of heteroatom-based co-doped biochar. To address this gap, this review gives a systematic analysis of co-doped biochar and its applications.

A bibliometric search conducted in the Web of Science database using the topic 'co-doped biochar' and 'dual-doped biochar' yielded 254 and 15 publications, respectively, from January 2018 to November 2024. Notably, the number of publications on co-doped biochar has gradually increased in recent years, as presented in Figure 1. Despite this growth, existing reviews lack a systematic evaluation of its preparation methods, physicochemical properties, and synergistic effects in adsorption and catalytic applications. Addressing these gaps is critical to unlock the full potential of heteroatom-based co-doped biochar in tackling environmental challenges.

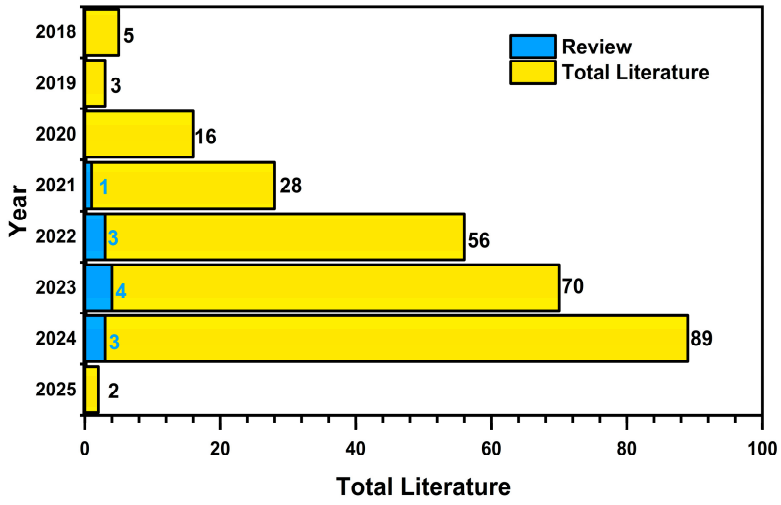

Figure 1. Yearly distribution of heteroatom-based co-doped biochar publications during 2018–2024.

To address the knowledge gap in the comprehensive research on heteroatom-based co-doped biochar as an adsorbent and catalyst, this review aims to provide an in-depth analysis through the following approaches: (1) employing bibliometric and knowledge visualization techniques to analyze the development trends in co-doped biochar over the past five years; (2) summarizing the synthesis methods and key physicochemical characteristics of heteroatom-based co-doped biochar; (3) elucidating its applications, along with an analysis of the mechanisms by which heteroatom-based co-doped biochar acts as an adsorbent and catalyst for contaminant removal; and (4) identifying notable research gaps, limitations, and challenges that must be addressed to advance the practical application of co-doped biochar.

2. Bibliometric Analysis of Publications on Co-Doped Biochar

To investigate the temporal distribution of keyword clusters, we examined the co-occurrence mapping of keywords over time, as depicted in Figure 2. To enhance the thematic progression analysis, a threshold of three was applied in the VOSviewer software (v. 1.8) for selected keywords at this stage. The timeline of the core keywords for 14 clusters and the initial occurrence time of the core keywords in each cluster are illustrated in Figure 3. As shown in Figures 2 and 3, a significant portion of research between 2020 and 2022 primarily focused on 'supercapacitor', 'catalysis', 'microbial fuel cells', and 'adsorption'. However, starting from 2023 to 2024, research on co-doped biochar had begun to focus on 'heteroatom doping' and 'Fe-N doping', indicating that heteroatom-based co-doped biochar has gradually become a prominent topic.

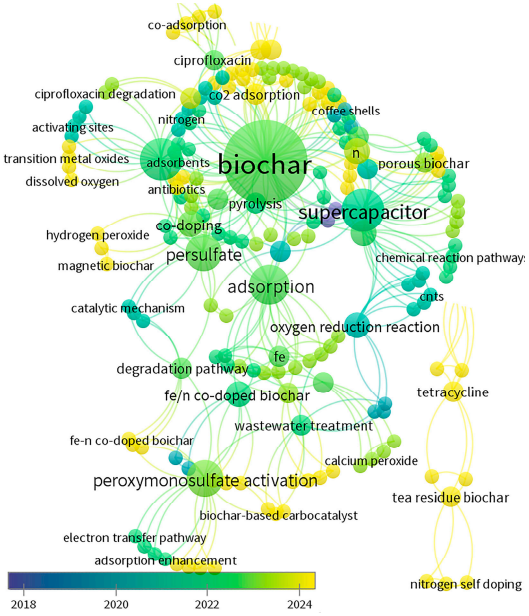

Figure 2. Temporal mapping of keyword co-occurrence in the study of 'co-doped biochar'.

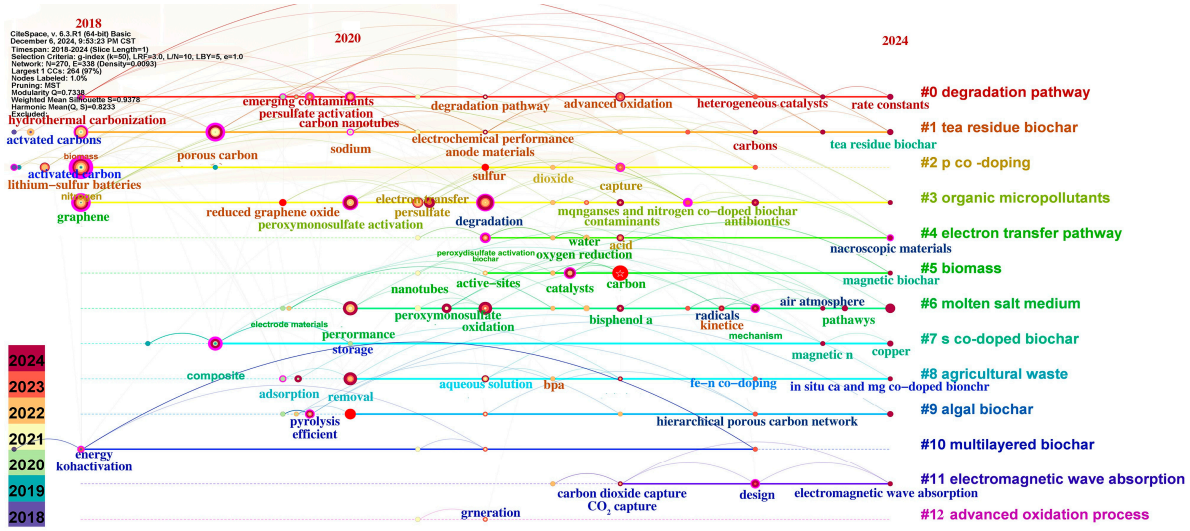

Figure 3. Timeline mapping of the clustering of research themes in 'co-doped biochar'.

3. Co-Doping Strategies

The available biomass from various waste sources, such as sewage sludge, wood, food residues, fruit skins, and straw, can be utilized as raw materials for the heteroatom-based co-doped biochar preparation. Typically, co-doping strategies for biochar based on heteroatoms typically can be divided into two categories: one-step and two-step processes (Figure 4). In the one-step synthesis method, simple co-pyrolysis of biomass feedstocks with doping precursors is conducted. The combination of pyrolysis with pre-doping or post-doping (physical or chemical) is performed as a two-step synthesis method, which involves carbonization and heteroatom doping during the preparation process. A summary of co-doping strategies is provided in Table 1.

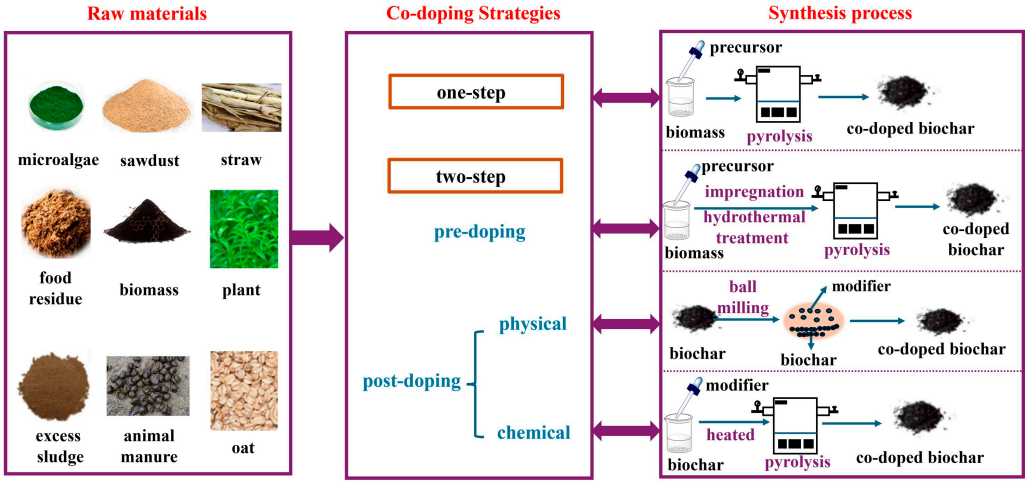

Figure 4. Schematic image of the preparation methods of heteroatom-based co-doped biochar.

Table 1. Doping strategies of heteroatom-based co-doped biochar.

Co-Doped				Biomass	Preparation	Activation/	Production	Application	Ref.
Doping Atoms	**Routes**	**Doping Methods**	**Element Feedstocks**	**Feedstocks**	**Conditions**	**Modification Regent**	**Atmosphere**		
Mg, N	pre-doping	impregnation–pyrolysis method	$MgCl_2·6H_2O$, NH_3	wheat straw and Douglas fir wood	impregnate with $MgCl_2·6H_2O$ solution, stir for 6 h, dry at 90 °C for 48 h, then pyrolyze under NH_3	NH_3	NH_3	phosphate adsorption	[16]
Co, N	post-doping	ligand-mediated method	metal acetate, o-phenanthroline	rice straw	mix with elemental precursors, evaporate at 60 °C for 4 h, then pyrolyze at 600 °C for 2 h under Ar		Ar	activate PMS for SMZ degradation	[17]
Co, N	one-step	pyrolysis method	$CoCl_2$, melamine	paulownia wood	mix with $CoCl_2$, melamine, and NaCl, then pyrolyze at 400 °C (5 °C/min, 1 h) and 900 °C (2 °C/min, 1 h) under N_2	HNO_3	N_2	cathode of Li-O_2 battery	[18]
Fe, N	pre-doping	impregnation–pyrolysis method	$FeCl_3·6H_2O$ and dicyandi-amide	sawdust	mix with $FeCl_3$ and dicyandiamide, stir and dry at 80 °C, then pyrolyze at 800 °C for 1 h under N_2		N_2	activate PMS to degrade BPA	[19]
Fe, N	pre-doping	impregnation–pyrolysis method	$FeCl_3·6H_2O$, NH_4NO_3	corn stalk	sonicate at 25 °C for 20 min, stir, then pyrolyze at 80 °C for 2 h and at 800 °C (1.5 °C/min, 1.5 h) under N_2		N_2	PDS activator for BPA degradation	[20]
Fe, N	pre-doping	impregnation–pyrolysis method	$CO(NH_2)_2$, $KHCO_3$, K_2FeO_4	corn straw	stir with dissolved urea for 9 h, mix with $KHCO_3$ and K_2FeO_4, then pyrolyze at 800 °C for 2 h under N_2		N_2	Cr(VI)and BPA removal	[21]
Fe, N	pre-doping	hydrothermal–pyrolysis method	$FeSO_4·7H_2O$, urea	wheat straw	mix with ascorbic acid, conduct hydrothermal reaction at 160 °C for 10 h, then pyrolyze at 800 °C (10 °C/min, 1 h) under N_2		N_2	activate PS for organic contaminant-degradation	[9]
B, N	post-doping	pyrolysis method	boric acid, urea	sawdust	mix with boric acid, seal with aluminum foil and pyrolyze at 800 °C (10 °C/min, 2 h), then repeat the same process to dope N		oxygen-deficient environment	activate PMS to remove CIP	[22]

Table 1. *Cont.*

Co-Doped				Biomass	Preparation	Activation/	Production	Application	Ref.
Doping Atoms	**Routes**	**Doping Methods**	**Element Feedstocks**	**Feedstocks**	**Conditions**	**Modification Regent**	**Atmosphere**		
B, N	pre-doping and post-doping	impregnation–pyrolysis method	boric acid, urea	wheat straw	dissolve with urea, stir at 70 °C until dry, then pyrolyze at 700 °C (10 °C/min, 1 h) under N_2, followed by pyrolysis with boric acid at 700 °C for 1 h		N_2	activate PDS for TC degradation	[23]
B, N	pre-doping	hydrothermal–impregnation–pyrolysis method	boric acid, urea	walnut shell	mix with hydrogen peroxide, glacial acetic acid, and water in a hydrothermal process at 120 °C for 5 h, impregnate with boric acid, urea, and walnut shell, then pyrolyze at 800 °C (3 °C/min, 3 h) under Ar		Ar	Au(III), Pt(IV), and Pd(II) adsorbent	[24]
Ce, N	pre-doping	impregnation–pyrolysis method	$Ce(NO_3)_3 \cdot 6H_2O$, urea	wheat straw pellets	stir mixture at 80 °C until dry, then pyrolyze at 500 °C for 3 h under N_2		N_2	CO_2 methanation catalysts	[25]
N, S	one-step	pyrolysis method	thiourea	lignin	pyrolyze at 700 °C (10 °C/min, 3 h)		N_2	activate CaO_2 for 4-nonylphenol degradation	[26]
N, S	post-doping	pyrolysis method	thiourea	peanut shell	pyrolyze at 200, 450 and 700 °C, then mix with thiourea and pyrolyze at 350 °C for 1 h, all under oxygen-limited conditions		oxygen-limited conditions	DEP adsorbent	[27]
N, S	one-step	pyrolysis method	urea, thiourea	sawdust	pyrolyze at 600, 700, and 800 °C (10 °C/min, 2 h)			activate PMS for gatifloxacin removal	[28]

Table 1. *Cont.*

Co-Doped				Biomass	Preparation	Activation/	Production	Application	Ref.
Doping Atoms	**Routes**	**Doping Methods**	**Element Feedstocks**	**Feedstocks**	**Conditions**	**Modification Regent**	**Atmosphere**		
N, S	pre-doping	impregnation–pyrolysis method	L-cysteine hydrochloride	cow dung	stir mixture at 80 °C for 4 h, dry at 60 °C for 48 h, then pyrolyze at 800 °C (5 °C/min, 2 h)			composite material foundation for TCH photocatalysis degradation	[29]
N, S	one-step	pyrolysis method		mantis shrimp shells	mix and pyrolyze at 750 °C	CO_2	CO_2	symmetric supercapacitor	[30]
N, O	pre-doping	hydrothermal–pyrolysis method	urea, $Zn(NO_3)_2{\cdot}6H_2O$	white pomelo peel	place mixture in autoclave at 95 °C for 6 h, dry at 120 °C in air, then pyrolyze at 500, 600, 700, and 800 °C for 2 h under N_2	H_2SO_4	N_2	supercapacitor electrode	[31]
Se, N	one-step	pyrolysis method	2,4,6-triselenocyanato-1,3,5-triazine	leaves of lemon verbena	grind with 2,4,6-triselenocyanato-1,3,5-triazine, then pyrolyze at 500 °C (20 °C/min, 2 h) under N_2		N_2	catalyst for aldehyde oxidation	[32]
Se, N	pre-doping	impregnation–pyrolysis method	NH_4Cl	Se-reducing bacterial cells	add NH_4Cl and freeze-dry mixture, then pyrolyze at 900 °C (5 °C/min, 2 h) under N_2		N_2	phenol adsorption and PMS activation	[33]

Note: SMZ: sulfamethoxazole, PDS: peroxydisulfate, BPA: bisphenol A, CIP: ciprofloxacin, PS: persulfate, TCH: tetracycline hydrochloride, TC: tetracycline, DEP: diethyl phthalate.

3.1. One-Step

In the one-step process, biomass is mechanically mixed with precursor materials containing doping element ions, followed by carbonization through heating under an inert gas environment at temperatures varying between 400 and 1000 °C. For instance, in a specific study, sawdust, urea, and thiourea were homogeneously mixed, and the dried sample was pyrolyzed at 600 °C for 2 h in an enclosed air atmosphere to produce N, S co-doped biochar [22]. In another example, Co, N co-doped biochar was synthesized from a mixture of paulownia wood pieces, NaCl, $CoCl_2$, and melamine [18]. The mixture was initially heated up to 400 °C with a heating rate of 5 °C/min, and kept for 1 h at this temperature, followed by continuing carbonization at 900 °C for 1 h. During the carbonization, the doping elements are incorporated into the carbon skeleton, meanwhile generating abundant pores and defect structures, which are advantages of the co-pyrolysis method due to its operational simplicity and time efficiency. However, the one-step method faces some challenges, like high energy requirements, severe self-assembly, and insufficient development of the pore structure in contrast to the two-step doping method [34–36].

3.2. Two-Step

3.2.1. Pre-Doping

The pre-doping method involves reacting raw biomass with sources of doping elements prior to carbonization. By employing impregnation or hydrothermal combination with pyrolysis processes, heteroatom-based co-doped biochar can be produced. For example, kelp powder was immersed in a solution of $Co(NO_3)_2{\cdot}6H_2O$ for 24 h, then the precipitate was isolated and heated at temperatures ranging from 600 to 900 °C in a tube furnace under an N_2 atmosphere with a heating rate of 10 °C/min for 3 h to obtain Co, N co-doped biochar [37]. From another study, microalgae powder was thoroughly mixed with $Fe(NO_3)_3{\cdot}9H_2O$ and urea solution. Then, this mixture was heated to 160 °C for 10 h to produce Fe, N co-doped biochar precursors, followed by pyrolysis at temperatures ranging from 500 to 800 °C for 2 h to produce Fe, N co-doped biochar [38]. Hydrothermal treatment facilitates the generation of abundant surface reactive oxygen functional groups in biomass [39]. Generally, impregnation pretreatment can effectively reduce ash content and increase the micro- and macro-porosity of biochar [40], while hydrothermal pretreatment can introduce additional functional groups to biochar under controlled reaction conditions [41]. However, the pre-doping method requires relatively longer production time due to impregnation or hydrothermal treatment. In addition, controlling the particle size and doping element content produced by pretreatment is challenging, and hydrothermal treatment may generate undesired byproducts [36] and require higher energy consumption.

3.2.2. Post-Doping

The post-modification of biochar often involves a two-step process in which biochar is first prepared, followed by the doping of target elements. In chemical post-modification, peanut shells were pyrolyzed at 200 to 700 °C under oxygen-limited conditions. Subsequently, pristine biochar and thiourea were annealed together in a muffle furnace at 350 °C for 1 h under an oxygen-limited environment to obtain N, S co-doped biochar [27]. Similarly, corncob-to-xylose residue was pyrolyzed at 400 °C for 2 h in a N_2 atmosphere to prepare pristine biochar, and then mixed with $MgCl_2{\cdot}6H_2O$ and heated at 120 °C for 2 h and 600 °C for another 2 h [16]. The heteroatom content and doping sequence play a crucial role in optimizing the functions of subsequent incorporated heteroatoms. In preparing N, B co-doped biochar, Choong et al. [42] observed that prior B doping in biochar can enhance N doping by enabling interactions between oxidized B and NH_3 during N doping, thus significantly enhancing the N doping pathway. N doping, particularly for graphitic-N, can

effectively activate conjugated π-electrons for peroxymonosulfate (PMS) activation and promote PMS adsorption, thus elevating the catalytic capacity of the biochar. Nevertheless, the excessive B introduction may create additional structural defective sites that hinder graphitic-N formation [22]. Therefore, the heteroatom content in the initial step is critical for regulating the biochar's catalytic performance. The processes of the heteroatom doping mechanism are shown in Figure 5.

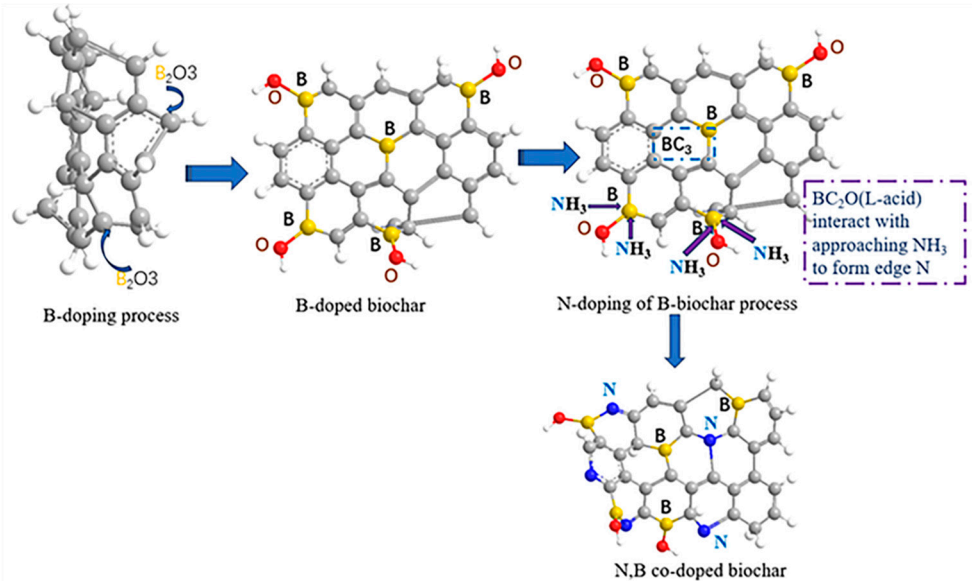

Figure 5. The schematic for the heteroatom doping mechanism, adapted from [22].

The chemical post-modification is relatively straightforward and easy to apply at a laboratory scale, offering excellent reduction and catalysis capabilities by increasing the biochar's surface area and functional groups. Additionally, post-modification facilitates the control of the size, shape, composition, and quantity of doping elements on the biochar. However, post-doping may lead to a decrease in heteroatom content due to potential instability in the heteroatom structure [43]. As for physical post-modification, ball milling is a feasible technique to fabricate co-doped biochar. Xie et al. [36] put forward a facile approach to anchor P onto N-doped biochar through ball milling at room temperature. They found that anchoring P onto the carbon skeleton via mechanical forces can effectively catalyze the degradation of diclofenac sodium. Ball milling offers lower operational costs, a more desirable biochar size distribution, and suitability for industrial applications. However, its initial cost is relatively high due to the substantial energy consumption and equipment requirements.

In general, both one-step and two-step fabrication methods possess distinct advantages and limitations. The physicochemical properties of co-doped biochar, including composition, particle size, and the quantity of doping elements, are influenced by the chosen fabrication method. Therefore, selecting an optimal fabrication method tailored to the available instruments and intended application is crucial.

4. Properties of Heteroatom-Based Co-Doped Biochar

4.1. Pore Volume and SSA

The pollutant removal efficiency is greatly affected by the distribution of pore size, SSA, and functional groups. In general, the pollutant removal performance of biochar is significantly enhanced when it exhibits an increased SSA and total pore volume. Table 2 presents the properties of heteroatom-based co-doped biochar. The pore size and SSA of biochar are strongly affected by factors such as the raw materials, pyrolysis temperature,

and the presence of heteroatoms. Due to the volatilization of water and other compounds during pyrolysis, biochar typically exhibits high porosity and a significantly large SSA. Generally, both pore volume and SSA increase with rising pyrolysis temperatures, though a decrease in the content of surface functional groups is often observed. Moreover, longer pyrolysis durations and lower heating rates can lead to an amplification in both pore size and pore volume within the biochar [44].

Table 2. Properties of heteroatom-based co-doped biochar.

Doping Atoms	Pore Size (nm)	S_{BET} (m^2/g)	Surface Functional Groups	Surface Defect	Ref.
Mg, N		167–536	pyridinic-N, pyridine-N, pyrrolic-N, graphitic-N, oxidized-N, C-O, C-N, C=C, C=O, C=N		[41]
Fe, N			$-NH_2^+$, $-NH_3^+$, C≡N, -COOH, -OH, Fe-O, C-OH, C=N		[35]
Fe, N		362.5	C=C, C-C, C-OH, C-N, C-O-C, C=O, C=N, Fe-O, C-OH, C=O	defect	[45]
Fe, N	4.2	473.72	Fe-O, C=O, Fe-O-C, C-C, C=O, pyridinic-N, Fe-N_X, pyrrolic-N, graphitic-N	defect	[46]
Fe, N		1691.81	C=C, C-H, Fe-O-C, C=N, Pyridinic-N, C=O	defect	[20]
Fe, N	3.414	234.7	-OH, N-H, $-CH_2$, $-CH_3$, C=N, C=O, C-C, C-OH, C=C, C-OH, C-O-C, C-N, Fe-O	defect	[47]
Fe, N	10	8	-NH, -OH, C-N, -C-H, C=C, C=O		[48]
Fe, N		130.720	C-C, Fe-O, C-H, C-O-C, -OH, -N/C-O-C, -CH, C=C, C-O/C-N, C=O/C-Fe	defect	[49]
Fe, N	3.414	133.6	graphitic-N, C-OH, C=N, $-CH_2$, $-CH_3$, C=N, C=O, C-C, C-OH, Fe-O, C=C, C-O-C	defect	[47]
Fe, Co	1.41	135.7	C-C, C=C, C-O, C-N, pyridinic-N, pyrrolic-N, graphitic-N, Co-N		[50]
Mn, N	1.994	923.7	C-C, C=C, C-O, C=O, π-π*, C-N, C-O-C, $-CH_2$-, $-CH_3$-, Mn-O, O=C-OH, pyridinic-N, pyrrolic-N, graphitic-N	defect	[51]
Se, N			C-H, C-N, -OH, -NH, C=N, C-C, C=C, C=O, C-O, O-C=O, $Se=C(NH_2)_2$, S-C		[32]
Se, N	0.207	287.25	C-Se-C, C-N, C-Se, C=O, O-C=O	defect	[33]
B, N			C-O-C, C=N, C-N, -NH, C-N-B, graphite-N, C=O, B-O, B_2O_3, BC_2O	defect	[52]
B, N		34.71	C-N, C-B, B-O, C=O, C-OH	defect	[23]
B, N		26.8–129.9	-OH, C=C, C-N, B-O, C-B, C-O, N-H		[22]
B, N	2.29	1011.81	C=C, C=O, O-H, C-O, B-C, C-N-B, B-N, B-CO_2	defect	[53]
N, S	3.79	125.9	O-H, N-H, C-H, C=O, O-C=O, C-O	carbon defects	[54]
N, S		107.7–372.9	C-O C-N C=C C=O C-H O-H C-S, π-π	defect	[38]
N, S	2–10	128.53	C-O, C-H, H-O-H, C=C, C-C, C-S, C-NC, -COOH, C-S-C, -C-SO_3-C-, -C-SO_2-C	defect	[55]
N, S			C=C, C-C, C-N, C-S, N-N, graphite-N, pyrrolic-N, pyridinic-N, C=O, C-O, C-OH, C-S-C, N-S-C		[26]

Table 2. *Cont.*

Doping Atoms	Pore Size (nm)	S_{BET} (m^2/g)	Surface Functional Groups	Surface Defect	Ref.
N, S			-OH, -NH, -C=CH_2, -C=O group, -C-N, C-S-C,	defect	[27]
N, S		40.64	C=N, C-S, C-S-C, C-N	defect	[49]
N, S		968–1109	pyridinic-N, pyrrolic-N, graphitic-N, oxides N, -C-S-C-, -C=S, -SO_X^- (x = 2–4)	defect	[56]
N, S	5.69–9.78	176–401	C-N, pyridinic-N, pyrrolic-N, graphitic-N, C-SOx-C (x = 3–4)	defect	[57]
N, O		50.1–1174.2	C-OH, C-H, N-H, -COO-, C=C, C=N, -NO_2, C-N, C-O, C=O, O-C=O, pyridinic-N, pyrrolic-N, graphitic-N, oxidized N		[58]
N, O	2	660	pyridinic-N, pyrrolic-N, graphitic-N, O-C=O, C-O, C=O		[59]
N, P	5.97–7.33	201–318	C-O-H, C-O-C, O-C=O, O-P-O, -N=C, -NH-, -N^+-		[60]
N, P		14.65–22.21	C=O, O-C=O, -OH, P-O, O-P-O, C=C, C-O, C-N, -OH, graphitic-N, pyrrolic-N, pyridinic-N, P=O, P-O		[61]
N, P	2.939	2675	C-C, C-N, C-O, P-O, P=O, P-C, C-O-C, C-N-C, C-N	defect	[20]
N, P	~1	248.3	P-O, P-C, N-C and P-C, pyridinic-N, pyrrolic-N, graphitic-N, oxidized N		[62]

Notably, the relationship between total pore volume, SSA, and pore size becomes considerably complex under high-temperature pyrolysis conditions when heteroatoms are involved in the reaction. For instance, Choong et al. [28] synthesized N, S co-doped biochar at various temperatures using a one-pot calcination protocol. They observed that SSA increased twelvefold from 34 m^2/g to 419 m^2/g when synthesis temperature increased from 600 to 800 °C. The introduction of heteroatoms into the biochar structure can result in a partial unblocking of obstructed pores, thereby increasing SSA. It was also noted that the pore volume of this N, S co-doped biochar at 700 °C (1.52 cm^3/g) was significantly higher than that at 800 °C (0.31 cm^3/g) due to the structural collapse of the pores within the biochar [28]. Conversely, when the pyrolysis temperature is below 400 °C, incomplete volatilization of certain constituents might lead to pore obstruction and hinder the development of new pores [47]. In general, a pyrolysis temperature range of 500–900 °C is considered optimal. However, higher SSA alone does not guarantee optimal removal performance, as additional characteristics of biochar should be considered, as discussed below.

4.2. Surface Functional Groups and Defects

The biochar's surface functional groups also play a vital role in contaminant removal. The distribution and type of functional groups on the biochar surface are influenced by the preparation method, temperature, raw material, and the presence of heteroatoms. The enrichment of oxygen- and heteroatom-containing functional groups determines the surface properties of biochar. Almost all types of heteroatom-based biochar contain functional groups, such as -OH, -COOH, and C=O, originating from the pristine biochar. However, the doping of heteroatoms can introduce many new functional groups, including graphitic-N, pyridinic-N, pyrrolic-N, -NH-, -N^+-, and O-P-O/P=O. Fan et al. [60] studied the Pb(II) adsorption by N, P co-doped biochar, finding that the removal capacity of Pb(II)

(723.6 mg/g) by this N, P co-doped biochar was significantly improved compared with the pristine biochar (264.2 mg/g). This study indicated that the chemical mechanism of the N, P co-doped biochar for Pb(II) removal involved surface complexation through N- and P-containing surface functional groups, including -N=C, -NH-, and O-P-O/P=O.

The addition of foreign atoms to the carbon structure, followed by partial evaporation at high temperature, generates newly formed topological intrinsic defects, classified as extrinsic defects [53]. Defective sites can create a 'localized state' within the delocalized π system, exhibiting distinct electronic and chemical properties that enhance the adsorption and catalytic activity of defective biochar compared to defect-free structures. The number of defects is highly dependent on the pyrolysis temperature. As the pyrolysis temperature increases, the potential for pore structure collapse grows, and foreign atoms escape, leading to increased defect formation. Han et al. [63] investigated the impact of pyrolysis temperature on defects in N, O co-doped biochar. The results suggested that the rapid loss of N atoms between 700 and 900 °C leads to the formation of numerous edge defects, whereas the rate of N atom loss slows, and graphitization accelerates between 900 and 1100 °C. Additionally, the number of defective sites is significantly influenced by activation methods and heteroatom concentrations [64]. Some studies have reported that introducing heteroatoms in co-doped biochar can form additional defective sites [31,65]. However, in another study, Fe, N co-doping was found to have a detrimental effect on defect formation compared to simple N-doping [58]. Therefore, the microscopic mechanism of defective sites in adsorption and catalytic activity requires further investigation.

5. The Environmental Applications of Heteroatom-Based Co-Doped Biochar

5.1. Adsorptive Pollutant Removal

Adsorption is a conventional method for pollutant removal due to several advantages, including its simple operation, high efficiency, and cost-effectiveness [35,66]. Recently, heteroatom-based co-doped biochar has emerged as a prospective alternative adsorbent due to its low cost and efficiency in removing considerable pollutants, including heavy metal ions (e.g., Cd(II), Cr(III), Sb(V)) [67–69], organic pollutants (ROPs) (e.g., DEP, bisphenol) [16,70], and inorganic substances (e.g., phosphate, CO_2) [16,65]. Moreover, co-doped biochar can maintain a high degree of graphitization and provide supplementary functional groups and structural defective sites, which promote its ability to remove pollutants.

5.1.1. Adsorptive Removal of Heavy Metal Ions

The pH of the initial solution significantly influences adsorption behavior due to the interspecies conversion of heavy metal ions and the presence of electroactive groups on the adsorbent surface. The best adsorption performance of heteroatom-based co-doped biochar typically occurs at pH values below neutral (Table 3), as protonation of the adsorbent under acidic conditions can attract more negatively charged metals. In contrast, heavy metal ions face increased competition with OH^- ions in alkaline conditions and are more likely to form precipitates [5,69,71].

Ionic strength is also an essential factor affecting the adsorption performance of heavy metal ions, as additional ions in solution will compete with the metal ions for limited adsorption sites. As for environmental wastewater, NaCl and $CaCl_2$ are the most representative ionic compounds; thus, the impact of ionic strength needs consideration in adsorption experiments. However, the total influence of ionic strength on heavy metal ion adsorption by heteroatom-based co-doped biochar is minimal, indicating a strong resistance to ionic strength interference [35,72]. This resilience may be attributed to the

abundant surface functional groups on heteroatom-based co-doped biochar, which combine with heavy metal ions to form complexes [72].

In addition, the dosage of biochar has a direct influence on adsorption capacity [73]. While increasing the amount of biochar can improve the efficiency of heavy metal ion adsorption, excessive amounts may lead to the overlapping of sorption layers, which block adsorption sites and subsequently reduce the adsorption capacity [74,75]. A study demonstrated that the adsorption efficiency of Cr(VI) increased with the Fe, N co-doped biochar dosage, achieving 99.9% removal efficiency within the first 10 min with an optimum dosage of 1.0 g/L [76].

Furthermore, the initial concentration of heavy metal ions also influences the adsorption behavior. Several studies have observed that adsorption capacity increases with higher initial concentrations, owing to the presence of unsaturated active sites on the biochar surface, eventually reaching equilibrium [24,76].

The typical adsorption performance and removal mechanism for heavy metal ions are summarized in Table 3. The adsorption mechanism of heavy metal ions onto heteroatom-based co-doped biochar depends on its surface functional groups, SSA, and the chemical nature of the heavy metal ions. Newly formed surface functional groups of the heteroatom-based co-doped biochar contribute to rapid adsorption rates and high adsorption capacities. Fan et al. [60] investigated the adsorption behavior of Pb(II) on heteroatom-based co-doped biochar enriched with N and P via the co-pyrolysis of Camellia oleifera shells. The adsorption capacity of this heteroatom-based co-doped biochar was 2.73 times higher than the pristine biochar. They observed that the formation of the N- and P-containing functional groups (-N=C, -NH-, -N^+-, and O-P-O/P=O) would facilitate the formation of strong chemical bonds with Pb(II).

Additionally, other mechanisms, including ligand exchange, hydrogen bonding, electrostatic attraction, and inner-sphere surface complexation, also exhibit favorable affinities towards heavy metals. Cao et al. [68] reported the remarkable adsorption capacity of Pb(II) (124.62 mg/g) and Cd(II) (57.71 mg/g) by Fe, S co-doped biochar. The presence of S-containing functional groups on Fe, S co-doped biochar was found to improve the uptake of Pb(II) and Cd(II) through chelation and ion exchange, while the iron-containing functional groups promoted adsorption via physical adsorption mechanisms.

Table 3. Adsorption performance and mechanism of heavy metal ions by heteroatom-based co-doped biochar.

Adsorbent	Heavy Metal Ions	Optimal pH	Adsorption Capacity	Adsorptive Mechanism	Ref.
N, P co-doped biochar	Pb(II)	6.0	723.6 mg/g	physisorption and chemical sorption	[60]
Ce, Fe co-doped biochar	Cd(II), Cr(III), Hg(II), and Pb(II)	neutral pH	18.60, 19.92, 49.64, and 13.69 mg/g	chemical/physical adsorptions	[77]
Fe, N co-doped biochar	Cr(VI)	2.0	99.9% of Cr(VI) removed within 10 min	adsorption, reduction, and complexation	[76]
B, N co-doped biochar	Au(III), Pt(IV), and Pd(II)	1, 4, and 3, resp.	246.96,108.80, and 44.78 mg/g	chemical adsorption	[35]
Fe, S co-doped biochar	Cd(II)/Pb(II)	unadjusted	57.71 mg/g and 124.62 mg/g	chelation, ion exchange, co-precipitation, and electrostatic interaction	[68]
Na, N co-doped biochar	Pb(II)/Cu(II)	5.0	959.6 and 299.1 mg/g	electrostatic interaction, ion exchange, complexation, and precipitation reactions	[78]

5.1.2. Adsorptive Removal of Organic Pollutants

The general adsorption performance and mechanism of organic pollutants are summarized in Table 4. The pH value of the solution affects both the properties of the adsorbent surface and the form of contaminant present in the solution. This makes pH a critical parameter influencing the organic pollutants' sorption behaviors of biochar, particularly when electrostatic interaction is the primary mechanism controlling the process.

Peng et al. [79] examined the role of solution pH in the adsorption behavior of CIP and norfloxacin (NOR) onto the Fe, N co-doped biochar. At pH < 6.0, the Fe, N co-doped biochar's surface carried a positive charge, while CIP and NOR existed in zwitterionic or neutral form. This enabled electrostatic attraction between the adsorbent and antibiotic molecules, leading to increased adsorption capacity. However, when pH > 6.0, the adsorption capacity decreased sharply. This decline was primarily attributed to CIP and NOR existing in their anionic or molecular forms, resulting in a greater degree of electrostatic repulsion between Fe, N co-doped biochar and these two antibiotics. In cases where electrostatic interaction is not the dominant mechanism, the adsorption performance of biochar is less sensitive to changes in solution pH. Xu et al. [16] studied the BPA adsorption on Fe, N co-doped biochar. The zeta potential of this biochar was 4.6, and at pH > 8.0 and pH > 10.0, BPA partially or fully undergoes deprotonation to BPA^- or $BPA_2{}^-$. Interestingly, the maximum adsorption capacity remained high even when the original pH of the solution was adjusted upwards to 10.4, suggesting no significant correlation between the surface charge properties of Fe, N co-doped biochar and its adsorption performance for BPA. Instead, π–π interactions between BPA and Fe, N co-doped biochar were identified as the dominant forces for adsorption.

Additionally, the co-existence of ions in solution will also influence the process of adsorption [80]. Common inorganic anions such as Na^+, K^+, Ca^{2+}, Mg^{2+}, Cl^-, $CO_3{}^{2-}$, $SO_4{}^{2-}$, $NO_3{}^-$, and $H_2PO_4{}^-$ exhibit a slight inhibition of the adsorption of ROPs by co-doped biochar [16,81]. This slight negative effect may result from competition between these co-existing ions and the target pollutants for the active adsorption sites on the biochar surface [16,82].

In comparison to heavy metal ions, organic molecules can play the role of a π–π electron donor and acceptor [5,83], interacting with functional groups (e.g., -OH, C=O) of the biochar surface. Moreover, the graphitized carbon (sp^2C) in biochar demonstrates a stronger potential to accept electrons, functioning as π-electron acceptors [61,84]. It has been proven that the sp^2C content and the electron acceptor capacity of biochar exhibit a positive relationship [61]. Doped heteroatoms play a crucial role in maintaining a high degree of graphitization, while also producing new functional groups that enhance chemical adsorption. Guo et al. [24] synthesized N, S co-doped biochar derived from peanut shells and observed that doping with N and S simultaneously resulted in the formation of new functional groups, including pyridinic-N and oxidized S. These functional groups exhibited improved adsorptive capability for DEP promotion, up to 14.34 mg/g. Ding et al. [61] demonstrated that a novel Fe, Mn, N co-doped biochar exhibited a higher adsorption capacity for bisphenol (84.96 mg/g) compared to the pristine biochar, single-element, and dual-element doped biochar. The Fe, Mn, and N co-doping maintained a high degree of graphitization, significantly improving the π–π electron–donor–acceptor (EDA) interactions, which were identified as the major mechanism driving bisphenol adsorption.

Table 4. Adsorptive behavior and mechanisms for removing organic pollutants using heteroatom-doped co-functional biochar.

Adsorbent	Organic Pollutants	Optimal pH	Adsorption Capacity	Adsorptive Mechanism	Ref.
N, S co-doped biochar	DEP	7.0	14.34 mg/g	Adsorption facilitated by abundant micropores and numerous active sites.	[27]
Fe, Zn co-doped biochar	p-nitrophenol	3.0	170 mg/g	Hydrophobic interaction.	[82]
Fe, Mn, N co-doped biochar	bisphenol	4.0	84.96 mg/g	A combination of EDA interaction, pore filling, electrostatic forces, hydrogen bonds, and hydrophobic effects.	[61]
Fe, N co-doped biochar	BPA	hardly affected	54 mg/g	EDA interactions.	[83]
Fe, N co-doped biochar	TC	unadjusted	156 mg/g	A mix of pore filling, electrostatic attractions, hydrogen bonding, surface complexation, and EDA interactions.	[33]
Fe, N co-doped biochar	NAP, ACE, and PHE	6.0	92.9, 56.3, and 83.1 mg/g, resp.	Adsorption via pore filling, π–π stacking interactions, mass transfer, and partition effects.	[85]
Fe, N co-doped biochar	NB	unadjusted	68.6 mg/g	Adsorption through chemical bonding, surface complexation, and reduction processes.	[86]
Fe, N co-doped biochar	RBR and MO	2.5 and 5.5	24.6 and 43.9 mg/g, resp.	Adsorption dominated by electrostatic attractions and ion exchange mechanisms.	[87]
Mn, N co-doped biochar	BPA	7.0	351 mg/g	Adsorption primarily driven by pore filling, hydrophobic forces, and EDA interactions.	[88]

Note: NAP: naphthalene, ACE: acenaphthene, PHE: phenanthrene, NB: nitrobenzene, RBR: reactive brilliant red K-2BP, MO: methyl orange.

5.1.3. Adsorption of Other Inorganic Substances

In addition to the contaminants discussed above, heteroatom-based co-doped biochar has also been utilized for the adsorption of other inorganic substances, such as CO_2 and phosphate. Mood et al. [16] developed N, Mg co-doped biochar with remarkable phosphate adsorption capacity, primarily attributed to the synergistic effect of N and Mg on the surface of the biochar, which improved phosphate adsorption. Similarly, Mg, N co-doped biochar derived from Douglas fir and chitosan demonstrated high phosphate adsorption efficiency of 112.4 mg PO_4^{3-} per gram of biochar, and the Langmuir and Freundlich isotherms confirmed both monolayer and heterogeneous adsorption mechanisms [89]. Wu et al. [90] designed N, S co-doped biochar with outstanding CO_2 capture capacities, achieving adsorptive uptake of 5.93 mmol/g at 0 °C and 3.83 mmol/g at 25 °C.

5.2. Activation Oxidation of Organic Pollutants as Activators

Advanced oxidation processes (AOPs) utilize radicals ($SO_4^{\bullet-}$, $^{\bullet}OH$, and $O_2^{\bullet-}$) as well as non-free radicals ($^1O_2$) to oxidize and decompose ROPs into intermediates or further into H_2O and CO_2. Heteroatom doping can induce non-radical ($^1O_2$) pathways, allowing the degradation of organic pollutants by AOPs to proceed primarily through a non-radical pathway or via a combination of both free radical and non-free radical routes within the catalytic process. Table 5 presents the performance of heteroatom-based co-doped biochar in the activation and oxidation of ROPs.

Zeng et al. [58] developed Fe, N co-doped biochar for PS activation in the degradation of TC, accomplishing a removal efficiency of 86.56% in 120 min. The results demonstrated that both free radicals and non-radical pathways participated in the degradation process. And the free radical pathway was confirmed to be associated with Fe doping; meanwhile, the non-radical pathway was predominantly influenced by N doping, specifically graphitic-N and pyridine-N. And the proposed catalytic mechanism is depicted in Figure 6.

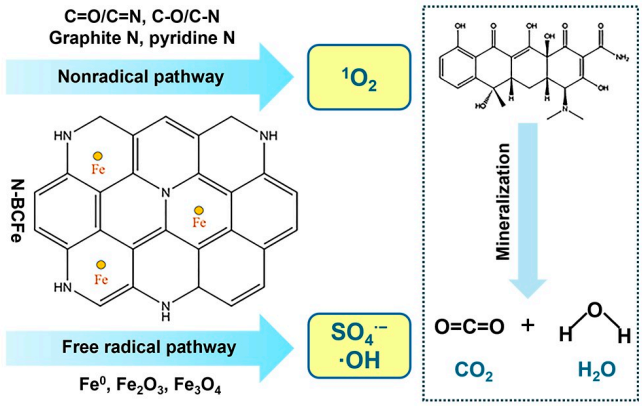

Figure 6. Diagrammatic representation of the TC degradation mechanism on the N-BCFe with PS activation, adapted from [45].

Zhang et al. [33] reported that Se, N co-doped biochar (Se/N-BC) exhibited a high phenol degradation efficiency of 99.2% within 5 min through a non-radical dominated pathway. The remarkable electron transfer features of Se/N-BC were due to the Se and N co-doping on the electron distribution within the carbon matrix demonstrating a synergistic regulation effect. This co-doping created an electronic transfer pathway, driving the non-radical oxidation. Choong et al. [22] investigated CIP removal using N, B co-doped biochar and identified that graphitic-N and BC_2O are the major active sites for PMS activation. Firstly, graphitic-N activated the conjugated π-electron system to facilitate PMS activation, while the co-existence of BC_3 functional groups with N functional groups further enhanced the total charge density of the biochar. Secondly, the co-doped N and B synergistically reduced the gap in energy levels between the HOMO and LUMO. Additionally, BC_2O and BCO_2 functioned as Lewis acid groups, promoting PMS adsorption/activation for $^1O_2$ formation. With these combined effects, the degradation efficiency for CIP removal reached approximately 80% within 60 min. The proposed activation mechanism for PMS is illustrated in Figure 7 [22].

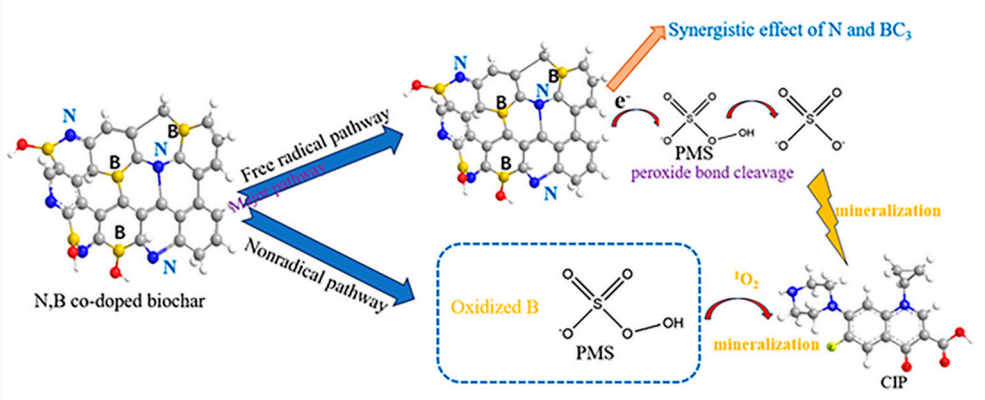

Figure 7. Illustration of the degradation mechanism for CIP by N, B co-doped biochar.

Zhang et al. [91] investigated the performance of N, S co-doped biochar for activating PDS in TCH degradation. Their findings revealed that the free radicals bound to the surface

and singlet oxygen ($^1O_2$) jointly contributed to TCH degradation. Moreover, pyrrolic-N and thiophene-S synergistically accelerated the process of electron transfer due to their close proximity to the Fermi level. The doping of thiophene-S induced localized positive charges in the material, thereby enhancing electron flow. Tang et al. [92] engineered N, P co-doped biochar for the removal of sulfonamides from complex aqueous solutions, demonstrating superior performance compared to AOP catalysts developed to date. Initially, the defect-containing graphitic structure of the co-doped biochar served as an electron transfer bridge, promoting PDS and H_2O to generate $HO_2^{\bullet-}$. Subsequently, the reaction of $S_2O_8^{2-}$ with $HO_2^{\bullet-}$ formed $O_2^{\bullet-}$ and $^{\bullet}OH$. The presence of P_2O_5 further enabled $O_2^{\bullet-}$ to act as a precursor for $^1O_2$, which played a dominant role in sulfonamide degradation.

The pH of the solution is a critical factor influencing both the catalytic degradation efficiency and the degradation pathway of ROPs. Xu et al. [38] explored the degradation of organic contaminants by the Fe, N co-doped biochar through PS activation. They found that $SO_4^{\bullet-}$ and $^{\bullet}OH$ dominated the BPA degradation process under both acidic and neutral conditions, whereas $^1O_2$ was the primary reactive species under alkaline conditions. In acidic conditions, Fe^{2+} promoted the generation of $SO_4^{\bullet-}$ and $^{\bullet}OH$. However, excess H^+ inhibited the transformation of $SO_4^{\bullet-}$ into $\bullet OH$, resulting in $SO_4^{\bullet-}$ becoming the dominant reactive species. In contrast, higher pH levels activated PMS to generate more $^1O_2$.

Furthermore, inorganic anions and natural organic compounds also affect degradation efficiency. Several studies proposed that the presence of inorganic anions and natural organic compounds would inhibit degradation [58,91], while others indicate no significant effect.

Table 5. Effectiveness of co-doped biochar containing heteroatoms in promoting the oxidative degradation of ROPs.

Activators	Oxidant	Pollutants	Performance	Mechanism	Ref.
B, N co-doped biochar	PMS	CIP	achieving CIP removal of 80% in 60 min	a combination of radical and non-radical pathways, with $SO_4^{\bullet-}$ dominating	[22]
N, S co-doped biochar	PMS	SMZ	97.84% of SMX can be degraded after 60 min	$SO_4^{\bullet-}$, $\bullet OH$, and $^1O_2$ were essential contributors to degradation	[55]
N, S co-doped biochar	PMS	gatifloxacin	achieving removal of almost 80% in 60 min	the non-radical pathways involving $^1O_2$ are dominant	[28]
N, S co-doped biochar	PMS	methylene blue	removal rate with k_{app} = 0.202 min^{-1}	the non-radical pathway	[93]
N, P co-doped biochar	PMS	diclofenac	the DS and TOC removal rates were 90.08% and 61.2%	rapid electron transfer	[94]
Co, N co-doped biochar	PMS	SMZ	degradation efficiency approach 99.6%	$SO_4^{\bullet-}$ and $^{\bullet}OH$ were the primary radicals involved	[17]
Co, N co-doped biochar	PMS	TC	degraded TC with a removal efficiency of 99% within 15 min	the degradation relied primarily on a non-radical mechanism	[37]
Co, S co-doped biochar	PMS	SMZ	SMX (20 mg/L) achieved complete degradation.	the process involved a synergy between free-radical and non-radical mechanisms	[95]

Table 5. *Cont.*

Activators	Oxidant	Pollutants	Performance	Mechanism	Ref.
Fe, N co-doped biochar	PMS	BPA	the mineralization rate of BPA was 68.9%	$SO_4^{\bullet-}$ and •OH were key under acidic/neutral conditions, while $^1O_2$ dominated under alkaline conditions	[19]
Se, N co-doped biochar	PMS	phenol	phenol achieved 99.2% removal in 5 min	a non-radical pathway	[33]
B, N co-doped biochar	PDS	TC	74.6% of TC can be eliminated in wastewater sample	electron transfer-dominated non-radical process	[23]
N, S co-doped biochar	PDS	TCH	TCH achieved an 85.6% removal efficiency in just 20 min	radicals $O_2^{\bullet-}$ and $^1O_2$ were critical in the degradation pathway	[91]
N, P co-doped biochar	PDS	sulfonamides	20 mg/L of sulfonamides was removed with a 98.33% efficiency in 120 min	the non-radical pathways involving $^1O_2$ are dominant	[92]
Cr, N co-doped biochar	PDS	TC	removal efficiency of 99.9% within 60 min	$^1O_2$-dominated pathway	[96]
N, S co-doped biochar	PS	AO7	removed 95.35% of the AO7 within 10 min	free radicals $SO_4^{\bullet-}$, O_2^-, and non-radical $^1O_2$ generated	[48]
Fe, N co-doped biochar	PS	SMZ	SMX achieved a high degradation efficiency of 98%	both free radical and non-free radical pathways are jointly involved	[38]
Fe, N co-doped biochar	PS	NOR	10 mg/L NOR achieved 95% degradation within 20 min	a co-dominance of radical and non-radical mechanisms was observed	[97]

Note: AO7: acid orange 7.

6. Future Perspectives

Synthesis and characteristic method improvement: The synthesis of heteroatom-based co-doped biochar is primarily achieved through one-step or two-step processes. However, these conventional methods often face limitations such as high energy consumption, inconsistent doping efficiency, and environmental concerns. To address these issues, green synthesis techniques have been proposed, but their application remains limited. For example, Sravanthi et al. [98] fabricated Fe^0 nanoparticles using a renewable extract of *Calotropis gigantea* flowers, which served as both reducing and stabilizing agents in a fully eco-friendly synthesis process to produce Fe^0, N co-doped biochar, highlighting the potential of green chemistry in this field. Future research should focus on further advancing green synthesis approaches by incorporating renewable resources and minimizing waste generation, thereby aligning with sustainability principles.

In addition, optimizing the synchronization of functional groups, pore structures, and defect sites is critical to enhancing the performance of heteroatom-based co-doped biochar. And further investigation into the synergistic effects at the micro-scale between heteroatoms, as well as between heteroatoms and the biochar matrix, is crucial to better understand and control the material's behavior during adsorption and catalytic processes. Advanced characterization techniques, such as atomic-resolution imaging and in situ spectroscopy, will be essential to uncover the synergistic effects between these structural

features during adsorption and catalytic processes. Such insights will drive the rational design of biochar with tailored properties for specific environmental applications.

Expanding applications of heteroatom-based co-doped biochar in environment remediation: Heteroatom-based co-doped biochar has demonstrated exceptional pollutant adsorption and catalytic degradation capabilities; however, most of these findings are limited to laboratory-scale experiments using synthetic solutions. To advance the practical application of heteroatom-based co-doped biochar, future research should investigate its performance under real-world conditions, such as natural soils and water systems, which present more complex and heterogeneous compositions. Expanding the scope of application to include soil remediation and nutrient recovery could provide significant benefits for sustainable agriculture and environmental restoration.

Additionally, the potential of heteroatom-based co-doped biochar to address global environmental challenges, including carbon storage and greenhouse gas emission reduction, warrants further exploration. Understanding the multifunctional roles of biochar in diverse environmental systems will enable the development of integrated solutions to address interrelated environmental challenges.

Disposal and stability of used biochar: Despite its growing application in pollutant removal, heteroatom-based co-doped biochar still faces significant challenges regarding its long-term use and disposal. One major concern is the potential release of heavy metal ions, which can lead to secondary pollution. For instance, Zhong et al. [99] reported that Cu ion release in the N-Cu/biochar/PS/TC system reached 3.29 ppm at pH 5.0, exceeding the permissible limits set by Chinese Environmental Protection Standards. These findings emphasize the urgent need for strategies to enhance biochar stability and mitigate the risks associated with its use.

Future research should focus on designing heteroatom-based co-doped biochar with improved stability to minimize environmental risks. Additionally, exploring sustainable disposal strategies, such as repurposing used biochar for construction materials or soil amendments, could provide viable end-of-life solutions. Comprehensive life-cycle assessments are also necessary to evaluate the environmental and economic impacts of biochar technologies, ensuring alignment with global sustainability goals.

7. Conclusions

This review summarizes the synthesis strategies, structural properties, and environmental applications of heteroatom-based co-doped biochar. Through the synergistic effects of heteroatoms, such as N, D, and P, co-doped biochar has demonstrated enhanced adsorption and catalytic performance for a variety of pollutants. Its significant advancements include increased functional groups, pore structures, and defect sites, which collectively improve its efficiency.

While laboratory results are promising, challenges such as stability, secondary pollution, and performance under complex environmental conditions remain. Future efforts should focus on optimizing green synthesis methods, advancing microscopic characterization, and developing sustainable disposal strategies to enable practical, large-scale applications. Heteroatom-based co-doped biochar holds significant potential for environmental remediation, with the potential for broader applications as research advances.

Author Contributions: Conceptualization, M.Y., S.L. and Y.W.; data curation, P.Z., writing—original draft preparation, M.Y.; writing—review and editing, S.L.; visualization, M.Y. and P.Z.; supervision, Y.W.; project administration, S.L. and Y.W.; funding acquisition, P.Z., S.L. and Y.W.; All authors have read and agreed to the published version of the manuscript.

Funding: This work is supported by the Zunyi Science and Technology Program Project (No. Zunshikehe HZ [2022]136), the Guizhou Provincial Science and Technology Projects (No. Qian Kehe Jichu (2022) normal 573), the innovation team project of Zunyi Normal University (No. [2024]06), the Special Key Laboratory of Electrochemistry for Materials of Guizhou Province (No. QJHKYZ [2018]004), and the Research Fund for the Doctoral Program of Zunyi Normal University (No. BS [2023]14).

Institutional Review Board Statement: Not applicable.

Informed Consent Statement: Not applicable.

Data Availability Statement: No new data were generated or analyzed in this study, and data sharing is not applicable to this article.

Conflicts of Interest: The authors declare no conflicts of interest.

References

1. Yang, L.J.; Liang, C.H.; Shen, F.; Hu, M.; Zhu, W.K.; Dai, L.C. A critical review on the development of lanthanum-engineered biochar for environmental applications. *J. Environ. Manag.* **2023**, *332*, 117318. [CrossRef] [PubMed]
2. Chen, Y.N.; Liu, Y.; Li, Y.P.; Wu, Y.X.; Chen, Y.R.; Zeng, G.M.; Zhang, J.C.; Li, H. Influence of biochar on heavy metals and microbial community during composting of river sediment with agricultural wastes. *Bioresour. Technol.* **2017**, *243*, 347–355. [CrossRef] [PubMed]
3. Liu, Y.H.; Chen, Y.N.; Li, Y.P.; Chen, L.; Jiang, H.J.; Li, H.; Luo, X.L.; Tang, P.; Yan, H.Q.; Zhao, M.Y. Fabrication, application, and mechanism of metal and heteroatom co-doped biochar composites (MHBCs) for the removal of contaminants in water: A review. *J. Hazard. Mater.* **2022**, *431*, 128584. [CrossRef] [PubMed]
4. Qu, J.H.; Shi, J.J.; Wang, Y.H.; Tong, H.; Zhu, Y.J.; Xu, L.S.; Wang, Y.F.; Zhang, B.; Tao, Y.; Dai, X. Applications of functionalized magnetic biochar in environmental remediation: A review. *J. Hazard. Mater.* **2022**, *434*, 128841. [CrossRef]
5. Wan, Z.H.; Yuqing, S.; Tsang, D.; Khan, E.; Ok, Y.S. Customised fabrication of nitrogen-doped biochar for environmental and energy applications. *Chem. Eng. J.* **2020**, *401*, 126136. [CrossRef]
6. Jalayeri, H.; Pepe, F. Novel and high-performance biochar derived from pistachio green hull biomass: Production, characterization, and application to Cu (II) removal from aqueous solutions. *Ecotoxicol. Environ. Saf.* **2019**, *168*, 64–71. [CrossRef] [PubMed]
7. Lee, M.-E.; Park, J.H.; Chung, J.W. Comparison of the lead and copper adsorption capacities of plant source materials and their biochars. *J. Environ. Manag.* **2019**, *236*, 118–124. [CrossRef] [PubMed]
8. RombolÀ, A.G.; Marisi, G.; Torri, C.; Fabbri, D.; Buscaroli, A.; Ghidotti, M.; Hornung, A. Relationships between chemical characteristics and phytotoxicity of biochar from poultry litter pyrolysis. *J. Agric. Food Chem.* **2015**, *63*, 6660–6667. [CrossRef] [PubMed]
9. Li, Z.; Chen, H.F.; Dong, C.Y.; Jin, C.Z.; Cai, M.Q.; Chen, Y.; Xie, Z.Q.; Xiong, X.G.Y.; Jin, M.C. Nitrogen doped bimetallic sludge biochar composite for synergistic persulfate activation: Reactivity, stability and mechanisms. *Environ. Res.* **2023**, *229*, 115998. [CrossRef] [PubMed]
10. Zhuang, M.; Wang, H.; Qi, L.; Cui, L.Q.; Quan, G.X.; Yan, J.L. Production of activated biochar via a self-blowing strategy-supported sulfidated nanoscale zerovalent iron with enhanced reactivity and stability for Cr(VI) reduction. *J. Clean. Prod.* **2021**, *315*, 128108. [CrossRef]
11. Mainali, K.; Mood, S.H.; Pelaez-Samaniego, M.R.; Sierra-Jimenez, V.; Garcia-Perez, M. Production and applications of N-doped carbons from bioresources: A review. *Catal. Today* **2023**, *423*, 114248. [CrossRef]
12. Xu, X.Y.; Zheng, Y.L.; Gao, B.; Cao, X.D. N-doped biochar synthesized by a facile ball-milling method for enhanced sorption of CO_2 and reactive red. *Chem. Eng. J.* **2019**, *368*, 564–572. [CrossRef]
13. Ye, Z.Z.; He, H.P.; Jiang, L. Co-doping: An effective strategy for achieving stable p-type ZnO thin films. *Nano Energy* **2018**, *52*, 527–540. [CrossRef]
14. Gao, Y.; Wang, Q.; Ji, G.z.; Li, A.M.; Niu, J.M. Doping strategy, properties and application of heteroatom-doped ordered mesoporous carbon. *RSC Adv.* **2021**, *11*, 5361–5383. [CrossRef]
15. Xiao, J.F.; Wang, Y.; Zhang, T.C.; Ouyang, L.K.; Yuan, S.J. Phytic acid-induced self-assembled chitosan gel-derived N, P-co-doped porous carbon for high-performance CO_2 capture and supercapacitor. *J. Power Sources* **2022**, *517*, 230727. [CrossRef]
16. Haghighi Mood, S.; Ayiania, M.; Cao, H.; Marin-Flores, O.; Milan, Y.J.; Garcia-Perez, M. Nitrogen and magnesium Co-doped biochar for phosphate adsorption. *Biomass Convers. Biorefin.* **2021**, *14*, 5923–5942. [CrossRef]
17. Gu, C.Y.; Zhang, Y.Q.; He, P.; Zhu, J.Y.; Gan, M. Insights into biochar supported atomically dispersed cobalt as an efficient peroxymonosulfate activator for sulfamethoxazole degradation: Robust performance, ROS and surface electron-transfer pathways. *Environ. Sci. Nano* **2022**, *9*, 3551–3561. [CrossRef]

18. Jing, S.Y.; Gai, Z.J.; Li, M.X.; Tang, S.F.; Ji, S.; Liang, H.G.; Chen, F.; Yin, S.B.; Tsiakaras, P. Enhanced electrochemical performance of a Li-O2 battery using Co and N co-doped biochar cathode prepared in molten salt medium. *Electrochim. Acta* **2022**, *410*, 140002. [CrossRef]
19. Xu, L.; Fu, B.R.; Sun, Y.; Jin, P.K.; Bai, X.; Jin, X.; Shi, X.; Wang, Y.; Nie, S.T. Degradation of organic pollutants by Fe/N co-doped biochar via peroxymonosulfate activation: Synthesis, performance, mechanism and its potential for practical application. *Chem. Eng. J.* **2020**, *400*, 125870. [CrossRef]
20. Wang, Y.J.; Wang, L.; Cao, Y.Q.; Bai, S.S.; Ma, F. Phase transformation-driven persulfate activation by coupled Fe/N–biochar for bisphenol a degradation: Pyrolysis temperature-dependent catalytic mechanisms and effect of water matrix components. *Environ. Pollut.* **2022**, *314*, 120296. [CrossRef]
21. Qu, J.H.; Zhang, X.B.; Liu, S.Q.; Li, X.J.; Wang, S.Y.; Feng, Z.H.; Wu, Z.H.; Wang, L.; Jiang, Z.; Zhang, Y. One-step preparation of Fe/N co-doped porous biochar for chromium(VI) and bisphenol a decontamination in water: Insights to co-activation and adsorption mechanisms. *Bioresour. Technol.* **2022**, *361*, 127718. [CrossRef] [PubMed]
22. Choong, Z.Y.; Gasim, M.F.; Zhou, T.; Hamidon, T.S.; Hussin, M.H.; Khoerunnisa, F.; Oh, W.-D. The influence of B heteroatom concentrations on the physiochemical properties of N, B-co-doped biochar for peroxymonosulfate activation in ciprofloxacin removal. *J. Water Process Eng.* **2023**, *51*, 103468. [CrossRef]
23. Dou, J.B.; Cheng, J.; Lu, Z.J.; Tian, Z.Q.; Xu, J.M.; He, Y. Biochar co-doped with nitrogen and boron switching the free radical based peroxydisulfate activation into the electron-transfer dominated nonradical process. *Appl. Catal. B* **2022**, *301*, 120832. [CrossRef]
24. Wang, Z.J.; Xu, X.W.; Ma, S.H.; Wang, H.; Zhao, H.; Wang, Y.; Tong, S.S.; Su, Z.; Wang, W.T.; Bai, J.B. The superior adsorption capacity of boron-nitrogen co-doping walnut shell biochar powder for Au (III), Pt (IV), and Pd (II). *J. Environ. Chem. Eng.* **2021**, *9*, 106288. [CrossRef]
25. Di Stasi, C.; Renda, S.; Greco, G.; González, B.; Palma, V.; Manyà, J.J. Wheat-Straw-Derived Activated Biochar as a Renewable Support of Ni-CeO_2 Catalysts for CO_2 Methanation. *Sustainability* **2021**, *13*, 8939. [CrossRef]
26. Dong, C.D.; Cheng, J.W.; Chen, C.W.; Huang, C.P.; Hung, C.M. Activation of calcium peroxide by nitrogen and sulfur co-doped metal-free lignin biochar for enhancing the removal of emerging organic contaminants from waste activated sludge. *Bioresour. Technol.* **2023**, *374*, 128768. [CrossRef] [PubMed]
27. Cui, J.L.; Zhang, F.; Li, H.Y.; Cui, J.G.; Ren, Y.T.; Yu, X.C. Recent Progress in Biochar-Based Photocatalysts for Wastewater Treatment: Synthesis, Mechanisms, and Applications. *Appl. Sci.* **2020**, *10*, 1019. [CrossRef]
28. Choong, Z.Y.; Gasim, M.F.; Lin, K.-Y.A.; Hamidon, T.S.; Hussin, H.; Oh, W.-D. Unravelling the formation mechanism and performance of nitrogen, sulfur codoped biochar as peroxymonosulfate activator for gatifloxacin removal. *Chem. Eng. J.* **2023**, *451*, 138958. [CrossRef]
29. Liu, Z.W.; Li, Y.; Li, C.; Thummavichai, K.; Feng, C.; Li, Z.; Liu, S.; Zhang, S.H.; Wang, N.N.; Zhu, Y.Q. MOF-derived biochar composites for enhanced high performance photocatalytic degradation of tetracycline hydrochloride. *RSC Adv.* **2022**, *12*, 31900–31910. [CrossRef] [PubMed]
30. Ding, Y.; Huang, S.Q.; Sun, Y.K.; Li, Y.C.; Zhu, L.J.; Wang, S.R. Preparation of Nitrogen and Sulfur Co-doped and Interconnected Hierarchical Porous Biochar by Pyrolysis of Mantis Shrimp in CO_2 Atmosphere for Symmetric Supercapacitors. *ChemElectroChem* **2021**, *8*, 3745–3754. [CrossRef]
31. Liang, G.W.; Yang, Z.; Wang, Z.W.; Cai, X.W.; Zhang, X.L.; Xie, X.Y. Relying on the non-radical pathways for selective degradation organic pollutants in Fe and Cu co-doped biochar/peroxymonosulfate system: The roles of Cu, Fe, defect sites and ketonic group. *Sep. Purif. Technol.* **2021**, *279*, 119697. [CrossRef]
32. Abedian-Dehaghani, N.; Sadjadi, S.; Heravi, M.M. Selenium and nitrogen co-doped biochar as an efficient metal-free catalyst for oxidation of aldehydes. *J. Mol. Struct.* **2022**, *1264*, 133237. [CrossRef]
33. Zhang, K.J.; Min, X.Y.; Zhang, T.Z.; Xie, M.B.; Si, M.Y.; Chai, L.Y.; Shi, Y. Selenium and nitrogen co-doped biochar as a new metal-free catalyst for adsorption of phenol and activation of peroxymonosulfate: Elucidating the enhanced catalytic performance and stability. *J. Hazard. Mater.* **2021**, *413*, 125294. [CrossRef]
34. Ho, S.H.; Zhu, S.S.; Chang, J.S. Recent advances in nanoscale-metal assisted biochar derived from waste biomass used for heavy metals removal. *Bioresour. Technol.* **2017**, *246*, 123–134. [CrossRef] [PubMed]
35. Ahmad, S.; Liu, L.A.; Zhang, S.C.; Tang, J.C. Nitrogen-doped biochar (N-doped BC) and iron/nitrogen co-doped biochar (Fe/N co-doped BC) for removal of refractory organic pollutants. *J. Hazard. Mater.* **2023**, *446*, 130727. [CrossRef] [PubMed]
36. Bhutto, A.W.; Qureshi, K.; Harijan, K.; Abro, R.; Abbas, T.; Bazmi, A.A.; Karim, S.; Yu, G. Insight into progress in pre-treatment of lignocellulosic biomass. *Energy* **2017**, *122*, 724–745. [CrossRef]
37. Zhu, H.; Guo, A.; Wang, S.M.; Long, Y.; Fan, G.Y.; Yu, X.J. Efficient tetracycline degradation via peroxymonosulfate activation by magnetic Co/N co-doped biochar: Emphasizing the important role of biochar graphitization. *Chem. Eng. J.* **2022**, *450*, 138428. [CrossRef]

38. Zhang, H.L.; Yan, Z.C.; Wan, J.Q.; Wang, Y.; Ye, G.; Huang, S.H.; Zeng, C.; Yi, J.X. Synthesis of Fe-Nx site-based iron-nitrogen co-doped biochar catalysts for efficient removal of sulfamethoxazole from water by activation of persulfate: Electron transfer mechanism of non-free radical degradation. *Colloids Surf. A* **2022**, *654*, 130174. [CrossRef]
39. Yin, Z.L.; Zhu, J.W.; Wang, Z.R.; Liu, Y.L.; Yang, Z.; Yang, W.B. Novel Fe/N co-doping biochar based electro-Fenton catalytic membrane enabling enhanced tetracycline removal and self-cleaning performance. *J. Clean. Prod.* **2023**, *402*, 136731. [CrossRef]
40. Alvarez, M.L.; Gasco, G.; Palacios, T.; Paz-Ferreiro, J.; Mendez, A. Fe oxides-biochar composites produced by hydrothermal carbonization and pyrolysis of biomass waste. *J. Anal. Appl. Pyrolysis* **2020**, *151*, 104893. [CrossRef]
41. Cheng, F.; Li, X.W. Preparation and Application of Biochar-Based Catalysts for Biofuel Production. *Catalysts* **2018**, *8*, 346. [CrossRef]
42. Wen, Q.; Chen, Y.J.; Rao, X.; Yang, R.; Zhao, Y.M.; Li, J.H.; Xu, S.Y.; Liang, Z.Y. Preparation of magnesium Ferrite-Doped magnetic biochar using potassium ferrate and seawater mineral at low temperature for removal of cationic pollutants. *Bioresour. Technol.* **2022**, *350*, 126860. [CrossRef]
43. Sun, Y.X.; Jia, J.X.; Huo, L.L.; Zhao, L.X.; Yao, Z.L.; Liu, Z.D. Heteroatom-doped biochar for CO_2 adsorption: A review of heteroatoms, doping methods, and functions. *Biomass Convers. Biorefin.* **2024**, *14*, 15237–15249. [CrossRef]
44. Wang, H.X.; Xu, J.L.; Sheng, L.X. Preparation of straw biochar and application of constructed wetland in China: A review. *J. Clean. Prod.* **2020**, *273*, 123131. [CrossRef]
45. Li, X.; Jia, Y.; Zhou, M.H.; Su, X.F.; Sun, J.H. High-efficiency degradation of organic pollutants with Fe, N co-doped biochar catalysts via persulfate activation. *J. Hazard. Mater.* **2020**, *397*, 122764. [CrossRef]
46. Li, X.; Zhang, S.X.; Yu, M.W.; Xu, H.; Lv, J.G.; Yang, S.S.; Zhu, X.T.; Li, L. One-pot pyrolysis method for synthesis of Fe/N co-doped biochar as an effective peroxymonosulfate activator for RhB degradation. *J. Taiwan Inst. Chem. Eng.* **2021**, *128*, 209–219. [CrossRef]
47. Leng, L.J.; Xiong, Q.; Yang, L.H.; Li, H.; Zhou, Y.Y.; Zhang, W.J.; Jiang, S.J.; Li, H.L.; Huang, H.J. An overview on engineering the surface area and porosity of biochar. *Sci. Total Environ.* **2021**, *763*, 144204. [CrossRef]
48. Wang, J.P.; Zhang, P.F.; Peng, J.X.; Zhang, Q.W.; Yao, J.; Wu, X.Y.; Li, Y.B. Sulfur and nitrogen co-doped magnetic biochar coupled with hydroxylamine for high-efficiency of persulfate activation and mechanism study. *Environ. Res.* **2023**, *216*, 114745. [CrossRef] [PubMed]
49. Wu, W.B.; Wang, R.P.; Chang, H.X.; Zhong, N.B.; Zhang, T.; Wang, K.; Ren, N.Q.; Ho, S.-H. Rational electron tunning of magnetic biochar via N, S co-doping for intense tetracycline degradation: Efficiency improvement and toxicity alleviation. *Chem. Eng. J.* **2023**, *458*, 141470. [CrossRef]
50. Wang, S.Z.; Wang, J.L. Bimetallic and nitrogen co-doped biochar for peroxymonosulfate (PMS) activation to degrade emerging contaminants. *Sep. Purif. Technol.* **2023**, *307*, 122807. [CrossRef]
51. Liu, Z.F.; He, M.; Tang, L.; Shao, B.B.; Liang, Q.H.; Wu, T.; Pan, Y.; Zhang, X.S.; Luo, S.H.; He, Q.Y.; et al. Dual redox cycles of Mn(II)/Mn(III) and Mn(III)/Mn(IV) on porous Mn/N co-doped biochar surfaces for promoting peroxymonosulfate activation and ciprofloxacin degradation. *J. Colloid Interface Sci.* **2023**, *634*, 255–267. [CrossRef] [PubMed]
52. Hung, C.-M.; Chen, C.-W.; Huang, C.-P.; Yang, Y.-Y.; Dong, C.-D. Suppression of polycyclic aromatic hydrocarbon formation during pyrolytic production of lignin-based biochar via nitrogen and boron co-doping. *Bioresour. Technol.* **2022**, *355*, 127246. [CrossRef] [PubMed]
53. Yang, S.J.; Xu, S.S.; Tong, J.Y.; Ding, D.H.; Wang, G.; Chen, R.Z.; Jin, P.K.; Wang, X.C.C. Overlooked role of nitrogen dopant in carbon catalysts for peroxymonosulfate activation: Intrinsic defects or extrinsic defects? *Appl. Catal. B* **2021**, *295*, 120291. [CrossRef]
54. Wang, S.Z.; Wang, J.L. Peroxymonosulfate activation by Co9S8@ S and N co-doped biochar for sulfamethoxazole degradation. *Chem. Eng. J.* **2020**, *385*, 123933. [CrossRef]
55. Xu, Y.; Liu, S.; Wang, M.; Zhang, J.; Ding, H.J.; Song, Y.Q.; Zhu, Y.; Pan, Q.X.; Zhao, C.; Deng, H.P. Thiourea-assisted one-step fabrication of a novel nitrogen and sulfur co-doped biochar from nanocellulose as metal-free catalyst for efficient activation of peroxymonosulfate. *J. Hazard. Mater.* **2021**, *416*, 125796. [CrossRef] [PubMed]
56. Yuan, H.R.; Zhao, Y.; Yang, J.Z.; Xiong, C.X.; Li, D.N.; Chen, Y. N, S-co-doping of activated biochar from herb residue for enhanced electrocatalytic performance toward oxygen reduction reaction. *J. Anal. Appl. Pyrolysis* **2022**, *166*, 105606. [CrossRef]
57. Huang, S.Q.; Ding, Y.; Li, Y.C.; Han, X.H.; Xing, B.; Wang, S.R. Nitrogen and Sulfur Co-doped Hierarchical Porous Biochar Derived from the Pyrolysis of Mantis Shrimp Shell for Supercapacitor Electrodes. *Energy Fuels* **2021**, *35*, 1557–1566. [CrossRef]
58. Zeng, H.P.; Li, J.X.; Xu, J.X.; Qi, W.; Hao, R.X.; Gao, G.W.; Lin, D.; Li, D.; Zhang, J. Preparation of magnetic N-doped iron sludge based biochar and its potential for persulfate activation and tetracycline degradation. *J. Clean. Prod.* **2022**, *378*, 134519. [CrossRef]
59. Cheng, B.H.; Deng, L.J.; Jiang, J.; Jiang, H. Catalytic cycloaddition of CO_2 to epoxides by the synergistic effect of acidity and alkalinity in a functionalized biochar. *Chem. Eng. J.* **2022**, *442*, 136265. [CrossRef]
60. Fan, Y.H.; Wang, H.; Deng, L.Y.; Wang, Y.; Kang, D.; Li, C.Z.; Chen, H. Enhanced adsorption of Pb (II) by nitrogen and phosphorus co-doped biochar derived from Camellia oleifera shells. *Environ. Res.* **2020**, *191*, 110030. [CrossRef] [PubMed]

61. Ding, H.; Zhang, Z.L.; Li, Y.; Ding, L.; Sun, D.X.; Dong, Z.Q. Fabrication of novel Fe/Mn/N co-doped biochar and its enhanced adsorption for bisphenol a based on π–π electron donor–acceptor interaction. *Bioresour. Technol.* **2022**, *364*, 128018. [CrossRef] [PubMed]
62. Ding, T.; Wu, Y.S.; Zhu, X.; Lin, G.Y.; Hu, X.; Sun, H.Q.; Huang, Y.; Zhang, S.; Zhang, H. Promoted Production of Phenolic Monomers from Lignin-First Depolymerization of Lignocellulose over Ru Supported on Biochar by N,P-co-Doping. *ACS Sustain. Chem. Eng.* **2022**, *10*, 2343–2354. [CrossRef]
63. Han, S.B.; Wu, Y.; Peng, S.M.; Xu, Y.Y.; Sun, M.; Su, X.H.; Zhong, Y.H.; Wen, H.L.; He, J.; Yu, L. Boosting the electrochemical performance of Zn-air battery with N/O co-doped biochar catalyst via a simple physical strategy of forced convection intensity. *Chem. Eng. Sci.* **2023**, *272*, 118615. [CrossRef]
64. Wang, D.; Dong, S.W.; Fu, S.Q.; Shen, Y.; Zeng, T.; Yu, W.T.; Lu, X.H.; Wang, L.Z.; Song, S.; Ma, J. Catalytic ozonation for imazapic degradation over kelp-derived biochar: Promotional role of N-and S-based active sites. *Sci. Total Environ.* **2023**, *860*, 160473. [CrossRef]
65. Yuan, X.F.; Xiao, J.F.; Yılmaz, M.; Zhang, T.C.; Yuan, S.J. N, P Co-doped porous biochar derived from cornstalk for high performance CO_2 adsorption and electrochemical energy storage. *Sep. Purif. Technol.* **2022**, *299*, 121719. [CrossRef]
66. Peiris, C.; Gunatilake, S.R.; Mlsna, T.E.; Mohan, D.; Vithanage, M. Biochar based removal of antibiotic sulfonamides and tetracyclines in aquatic environments: A critical review. *Bioresour. Technol.* **2017**, *246*, 150–159. [CrossRef]
67. Zhou, Z.K.; Bu, Y.; Long, X.L.; Cai, J.J. N-containing biochar from oatmeal: Hydrothermal synthesis and used as highly efficient adsorbent for Cr (VI) adsorptive-reduction removal. *Biomass Convers. Biorefin.* **2023**, *14*, 19519–19528. [CrossRef]
68. Cao, B.; Qu, J.H.; Yuan, Y.H.; Zhang, W.H.; Miao, X.M.; Zhang, X.R.; Xu, Y.; Han, T.Y.; Song, H.J.; Ma, S.Y. Efficient scavenging of aqueous Pb (II)/Cd (II) by sulfide-iron decorated biochar: Performance, mechanisms and reusability exploration. *J. Environ. Chem. Eng.* **2022**, *10*, 107531. [CrossRef]
69. Wang, L.; Wang, J.Y.; Wang, Z.X.; Feng, J.T.; Li, S.S.; Yan, W. Synthesis of Ce-doped magnetic biochar for effective Sb(V) removal: Performance and mechanism. *Powder Technol.* **2019**, *345*, 501–508. [CrossRef]
70. Guo, R.S.; Yan, L.L.; Rao, P.H.; Wang, R.K.; Guo, X. Nitrogen and sulfur co-doped biochar derived from peanut shell with enhanced adsorption capacity for diethyl phthalate. *Environ. Pollut.* **2019**, *258*, 113674. [CrossRef]
71. Mao, W.; Zhang, Y.; Luo, J.E.; Chen, L.T.; Guan, Y.T. Novel co-polymerization of polypyrrole/polyaniline on ferrate modified biochar composites for the efficient adsorption of hexavalent chromium in water. *Chemosphere* **2022**, *303*, 135254. [CrossRef]
72. Pan, J.; Deng, H.W.; Du, Z.Y.; Tian, K.; Zhang, J.F. Design of nitrogen-phosphorus-doped biochar and its lead adsorption performance. *Environ. Sci. Pollut. Res.* **2022**, *29*, 28984–28994. [CrossRef] [PubMed]
73. Ihsanullah, I.; Khan, M.T.; Zubair, M.; Bilal, M.; Sajid, M. Removal of pharmaceuticals from water using sewage sludge-derived biochar: A review. *Chemosphere* **2022**, *289*, 133196. [CrossRef] [PubMed]
74. Singh, S.; Kumar, V.; Dhanjal, D.S.; Datta, S.; Bhatia, D.; Dhiman, J.; Samuel, J.; Prasad, R.; Singh, J. A sustainable paradigm of sewage sludge biochar: Valorization, opportunities, challenges and future prospects. *J. Clean. Prod.* **2020**, *269*, 122259. [CrossRef]
75. Zhang, L.J.; Zhang, X.; Liang, H.F.; Xie, Y.; Tao, H.C. Ammonium removal by a novel magnetically modified excess sludge. *Clean Technol. Environ. Policy* **2018**, *20*, 2181–2189. [CrossRef]
76. Zhang, Y.T.; Liu, N.; Yang, Y.D.; Li, J.L.; Wang, S.C.; Lv, J.; Tang, R. Novel carbothermal synthesis of Fe, N co-doped oak wood biochar (Fe/N-OB) for fast and effective Cr (VI) removal. *Colloids Surf. A* **2020**, *600*, 124926. [CrossRef]
77. Maneechakr, P.; Mongkollertlop, S. Investigation on adsorption behaviors of heavy metal ions (Cd 2+, Cr 3+, Hg 2+ and Pb 2+) through low-cost/active manganese dioxide-modified magnetic biochar derived from palm kernel cake residue. *J. Environ. Chem. Eng.* **2020**, *8*, 104467. [CrossRef]
78. Fu, M.Y.; Ma, Q.H.; Luo, Y.; Feng, W.; Wang, X.H. Na/N Co-doped Seaweed Biochar Composite for Efficient Removal of Aqueous Pb(II) and Cu(II). *Chem. Asian J.* **2024**, *19*, e202400163. [CrossRef]
79. Peng, X.M.; Hu, F.P.; Zhang, T.; Qiu, F.X.; Dai, H.L. Amine-functionalized magnetic bamboo-based activated carbon adsorptive removal of ciprofloxacin and norfloxacin: A batch and fixed-bed column study. *Bioresour. Technol.* **2017**, *249*, 924–934. [CrossRef]
80. Yang, C.; Wu, S.C.; Cheng, J.H.; Chen, Y.C. Indium-based metal-organic framework/graphite oxide composite as an efficient adsorbent in the adsorption of rhodamine B from aqueous solution. *J. Alloys Compd.* **2016**, *687*, 804–812. [CrossRef]
81. Mei, Y.L.; Xu, J.; Zhang, Y.; Li, B.; Xu, H.C. Effect of Fe–N modification on the properties of biochars and their adsorption behavior on tetracycline removal from aqueous solution. *Bioresour. Technol.* **2021**, *325*, 124732. [CrossRef]
82. Wang, P.; Tang, L.; Wei, X.; Zeng, G.M.; Zhou, Y.Y.; Deng, Y.C.; Wang, J.J.; Xie, Z.H.; Fang, W. Synthesis and application of iron and zinc doped biochar for removal of p-nitrophenol in wastewater and assessment of the influence of co-existed Pb(II). *Appl. Surf. Sci.* **2017**, *392*, 391–401. [CrossRef]
83. Xu, L.; Wu, C.X.; Chai, C.; Cao, S.Y.; Bai, X.; Ma, K.Y.; Jin, X.; Shi, X.; Jin, P.K. Adsorption of micropollutants from wastewater using iron and nitrogen co-doped biochar: Performance, kinetics and mechanism studies. *J. Hazard. Mater.* **2022**, *424*, 127606. [CrossRef] [PubMed]

84. Sun, Z.Q.; Zhao, L.; Liu, C.H.; Zhen, Y.F.; Ma, J. Fast adsorption of BPA with high capacity based on π-π electron donor-acceptor and hydrophobicity mechanism using an in-situ sp2 C dominant N-doped carbon. *Chem. Eng. J.* **2020**, *381*, 122510. [CrossRef]
85. Cheng, H.; Ji, R.; Bian, Y.; Jiang, X.; Song, Y. From macroalgae to porous graphitized nitrogen-doped biochars—Using aquatic biota to treat polycyclic aromatic hydrocarbons-contaminated water. *Bioresour. Technol.* **2020**, *303*, 122947. [CrossRef] [PubMed]
86. Song, W.; Gao, B.; Xu, X.; Xing, L.; Han, S.; Duan, P.; Song, W.; Jia, R. Adsorption-desorption behavior of magnetic amine/Fe_3O_4 functionalized biopolymer resin towards anionic dyes from wastewater. *Bioresour. Technol.* **2016**, *210*, 123–130. [CrossRef] [PubMed]
87. Ahmad, S.; Gao, F.; Lyu, H.; Ma, J.; Zhao, B.; Xu, S.; Ri, C.; Tang, J. Temperature-dependent carbothermally reduced iron and nitrogen doped biochar composites for removal of hexavalent chromium and nitrobenzene. *Chem. Eng. J.* **2022**, *450*, 138006. [CrossRef]
88. Wu, W.L.; Zhang, J.W.; Zhu, W.J.; Zhao, S.H.; Gao, Y.C.; Li, Y.; Ding, L.; Ding, H. Novel manganese and nitrogen co-doped biochar based on sodium bicarbonate activation for efficient removal of bisphenol A: Mechanism insight and role analysis of manganese and nitrogen by combination of characterizations, experiments and density functional theory calculations. *Bioresour. Technol.* **2024**, *399*, 130608. [CrossRef]
89. Mainali, K.; Mullen, C.A.; Sarker, M.I.; Haghighi Mood, S.; Garcia-Perez, M. Production of N–Mg doped biochars for phosphate adsorption from renewable sources. *Biomass Bioenergy* **2024**, *185*, 107221. [CrossRef]
90. Wu, W.J.; Wu, C.L.; Liu, J.; Yan, H.Y.; Li, G.Q.; Zhao, Y.Q.; Bei, K.L.; Zhang, G.J. Synergistic effects of heteroatom doping and narrow micropores on carbon dioxide capture in bamboo shoot shell-based porous carbon. *Sep. Purif. Technol.* **2024**, *339*, 126690. [CrossRef]
91. Zhang, H.D.; Li, L.J.; Li, Y.J.; He, R.; Li, H.Y.; Yu, Y. N and S co-doped pine needle biochar activated peroxydisulfate for antibiotic degradation. *J. Clean. Prod.* **2022**, *379*, 134619. [CrossRef]
92. Tang, W.; Alessi, D.S.; Wang, T.; Wu, J.Q.; Li, S.J.; Konhauser, K.O.; Li, Z.X.; Chen, J.W. Efficient removal of sulfonamides in complex aqueous environments by an N, P-co-doped graphitic biochar: The crucial role of P_2O_5. *Green Chem.* **2024**, *26*, 3229–3238. [CrossRef]
93. Oh, W.-D.; Zaeni, J.R.J.; Lisak, G.; Lin, K.-Y.A.; Leong, K.-H.; Choong, Z.-Y. Accelerated organics degradation by peroxymonosulfate activated with biochar co-doped with nitrogen and sulfur. *Chemosphere* **2021**, *277*, 130313. [CrossRef] [PubMed]
94. Xie, J.; Xu, P.F.; Liu, M.H.; Liu, Y.L.; Zhu, L.; Yu, F.X.; Zhang, P.K.; Li, J.; Luo, Y.F.; Zhou, B. Anchoring phosphorus on in-situ nitrogen-doped biochar by mechanical milling for promoted electron transfer from diclofenac sodium to peroxymonosulfate. *Sep. Purif. Technol.* **2022**, *301*, 121964. [CrossRef]
95. Huang, X.Y.; Yu, Z.D.; Shi, Y.B.; Liu, Q.S.; Fang, S.Q. Highly efficient activation of peroxymonosulfate by Co, S co-doped bamboo biochar for sulfamethoxazole degradation: Insights into the role of S. *J. Environ. Chem. Eng.* **2022**, *10*, 108380. [CrossRef]
96. Guo, L.J.; Zhao, L.M.; Cheng, X.; Tang, Y.L.; Zhou, J.F.; Shi, B. Cr and N co-doped biochar driving controllable peroxydisulfate activation pathways to degrade tetracycline: Pyrrolic N inducing singlet oxygen generation. *Chem. Eng. J.* **2024**, *485*, 149294. [CrossRef]
97. Xi, M.F.; Cui, K.P.; Cui, M.S.; Ding, Y.; Guo, Z.; Chen, Y.H.; Li, C.X.; Li, X.Y. Enhanced norfloxacin degradation by iron and nitrogen co-doped biochar: Revealing the radical and nonradical co-dominant mechanism of persulfate activation. *Chem. Eng. J.* **2021**, *420*, 129902. [CrossRef]
98. Sravanthi, K.; Ayodhya, D.; Yadgiri Swamy, P. Green synthesis, characterization of biomaterial-supported zero-valent iron nanoparticles for contaminated water treatment. *J. Anal. Sci. Technol.* **2018**, *9*, 3. [CrossRef]
99. Zhong, Q.F.; Lin, Q.T.; Huang, R.L.; Fu, H.Y.; Zhang, X.F.; Luo, H.Y.; Xiao, R.B. Oxidative degradation of tetracycline using persulfate activated by N and Cu codoped biochar. *Chem. Eng. J.* **2020**, *380*, 122608. [CrossRef]